City Research Online

City St George's, University of London

Citation: Morny, E., Patel, K., Votruba, M., Binns, A. M. & Margrain, T. H. (2019). The Relationship Between the Photopic Negative Response and Retinal Ganglion Cell Topography. Investigative Ophthalmology and Visual Science, 60(6), pp. 1879-1887. doi: 10.1167/iovs.18-25272

This is the published version of the paper.

This version of the publication may differ from the final published version. To cite this item please consult the publisher's version.

Permanent repository link: https://openaccess.city.ac.uk/id/eprint/22197/

Link to published version: https://doi.org/10.1167/iovs.18-25272

Copyright and Reuse: Copyright and Moral Rights remain with the author(s) and/or copyright holders. Copies of full items can be used for personal research or study, educational, or not-for-profit purposes without prior permission or charge, unless otherwise indicated, provided that the authors, title and full bibliographic details are credited, a hyperlink and/or URL is given for the original metadata page and the content is not changed in any way. For full details of reuse please refer to City Research Online policy.

City Research Online: http://openaccess.city.ac.uk/ publications@citystgeorges.ac.uk

The Relationship Between the Photopic Negative Response and Retinal Ganglion Cell Topography

Enyam Komla A. Morny,[1] Kishan Patel,[2] Marcela Votruba,[2,3] Alison M. Binns,[4] and Tom H. Margrain[2]

[1]Department of Optometry and Vision Science, University of Cape Coast, Cape Coast, Ghana
[2]School of Optometry and Vision Sciences, Cardiff University, Cardiff, Wales, United Kingdom
[3]Eye Unit, University Hospital of Wales, Cardiff, Wales, United Kingdom
[4]School of Health Sciences, City, University of London, London, United Kingdom

Correspondence: Tom H. Margrain, School of Optometry and Vision Sciences, Cardiff University, Maindy Road, Cardiff, Wales CF24 4HQ, UK; MargrainTH@cardiff.ac.uk.

Submitted: July 30, 2018
Accepted: February 21, 2019

Citation: Morny EKA, Patel K, Votruba M, Binns AM, Margrain TH. The relationship between the photopic negative response and retinal ganglion cell topography. *Invest Ophthalmol Vis Sci*. 2019;60:1879–1887. https://doi.org/10.1167/iovs.18-25272

Purpose. To assess the topographic relationship between the photopic negative response (PhNR) and retinal ganglion cell distribution in healthy individuals.

Method. Data was recorded from 16 healthy participants. The amplitude of PhNRs obtained in response to focal long duration (250 ms) and brief flash (5 ms), red (660 nm) on blue (469 nm) stimuli of increasing size (5° – full field) were measured. The number of retinal ganglion cell receptive fields (RGCf) in each stimulus area was established from the literature and regression analysis used to determine the relationships between: PhNR amplitude and number of RGCfs stimulated, PhNR density and the RGCf density and response per RGCf as a function of eccentricity.

Results. The overall amplitude of the PhNR increased with stimulus size and the response density declined from ~0.1 μV/deg in the macular region to ~0.003 μV/deg approximately 45° from the fovea. Contrary to expectations, the relationship between the PhNR and number of RGCf was nonlinear, the response from more eccentric neurons being about three times greater than those in the macular region.

Conclusions. Although the amplitude of the PhNR broadly maps on to the topographic distribution of RGCf the increase in PhNR amplitude with increasing eccentricity is only partly explained by RGCf numbers. Increases in the PhNR amplitude may be due to topographic variations in the contributions from other non-RGC neurons, as well as eccentricity-related morphologic and physiologic differences in RGCs.

Keywords: photopic negative response, retinal ganglion cells, receptive fields, d-wave, electrophysiology

The photopic negative response (PhNR) is a negative going wave seen after the b-wave in a brief-flash photopic (cone) ERG.[1,2] The PhNR, particularly when elicited by a red flash on a rod saturating blue background, is believed to originate primarily from retinal ganglion cells (RGCs).[1–4] When a long-duration flash is used the PhNR is seen once after the b-wave (PhNR-ON) and again as a negative going wave after the d-wave (PhNR-OFF). The PhNR-ON and PhNR-OFF are thought to reflect the activity of the ON- and OFF-RGC pathways respectively.[3,5]

Simplistically, one might expect to find a linear relationship between RGC cell numbers and PhNR amplitude but several lines of evidence suggest this may not be the case. In pharmacologic experiments in macaque to establish the origins of the PhNR,[3] and in animal studies of glaucoma,[2,5] residual PhNR amplitudes are observed in the absence of RGC activity. Furthermore, studies attempting to correlate PhNR amplitude loss with structural or functional losses in the RGC complex and/or nerve fiber layer show that central RGC losses produce significant amplitude losses in the focal PhNR,[6–8] but not always in the full-field PhNR.[9,10] On the other hand, diffuse or peripheral RGC losses show more prominent attenuation of the full-field PhNR amplitude.[9,11] Despite the fact that the full field and focal PhNR are being used clinically in the diagnosis and monitoring of glaucoma and other diseases[12] the assumption that a given reduction in PhNR amplitude corresponds with a similar reduction in RGC cell count is questionable.

Hence, the overarching aim of this study was to better understand the relationship between RGC cell numbers and PhNR amplitude as a function of retinal eccentricity. Given that the relationship may be pathway dependent brief and long duration stimuli were used to tease apart any ON/OFF pathway differences. Furthermore, since RGC cell bodies can be displaced, particularly in the central retina, the estimates of the number of RGC stimulated by a given field size were based on the elegant RGC receptive fields (RGCf) modelling approach developed by Watson.[13]

Methods

Participants

Participants were recruited from among staff and students of the School of Optometry and Vision Sciences, Cardiff University, as well as their friends and families. All participants had a corrected visual acuity of 0.1 logMAR or better with normal visual fields and no underlying ocular or systemic conditions. The study conformed to the tenets of the Declaration of

Copyright 2019 The Authors

This work is licensed under a Creative Commons Attribution-NonCommercial-NoDerivatives 4.0 International License.

Downloaded from arvojournals.org on 05/13/2019

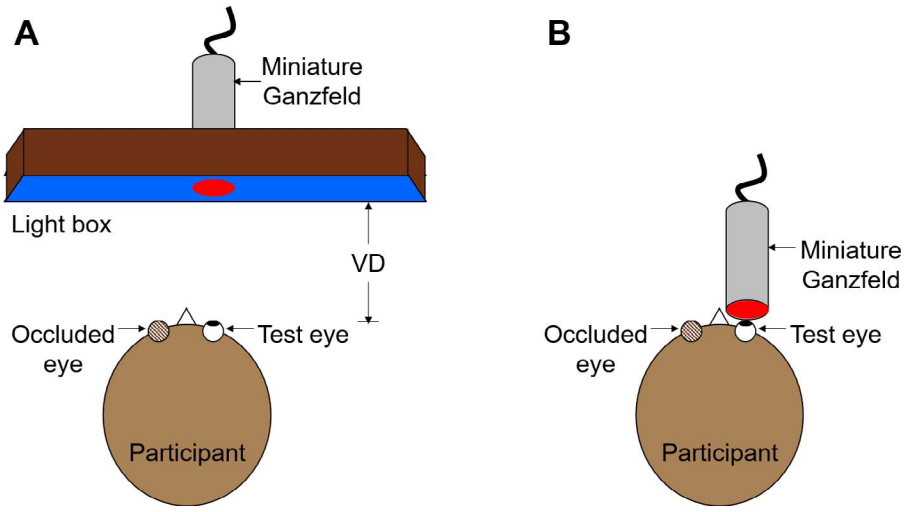

FIGURE 1. Schematic diagram showing the positions of the participant and the stimulus for recording focal ERGs (**A**) and full-field ERGs (**B**). Angular diameter of the stimulus was obtained by varying the VD. Note that the rod saturating *blue background* was on constantly with the flashing red stimulus superimposed on the *blue background*.

Helsinki and was approved by the ethics committee of the School. All participants provided their written consent after receiving a participant information sheet and having the opportunity to ask questions.

ERG Recording and Participant Setup

ERGs were recorded monocularly using DTL fiber electrodes (Unimed Electrode Supplies, Ltd., Surrey, UK) as active and contralateral reference electrodes. The DTL fiber was placed in the lower fornix to maximize stability during recording and the loose end fastened using medical tape at the inner canthus (Blenderm, Viasys Healthcare Ltd., Warwick, UK). A silver-silver chloride 10-mm diameter touch-proof skin electrode (Unimed Electrode Supplies, Ltd.), placed at the midfrontal forehead position was used as ground electrode. The pupils of participants were dilated using 1% tropicamide to a minimum of 7 mm.

All ERG responses were elicited using a miniature Ganzfeld LED stimulator (CH Electronics, Bromley, Kent, UK) and recorded on a commercial system (Medelec Synergy; Oxford Instruments PLC, Surrey, UK). Responses were bandpass filtered from 1 to 100 Hz and digitally averaged at a sampling rate of 1000 Hz. Signals were recorded in blocks of 10 to 20 responses, with a total of 40 to 60 averaged per trace. Between 4 and 6 traces were obtained for each stimulus condition. The traces were superimposed to confirm signal repeatability and averaged offline into a single averaged trace containing 160 to 300 responses. An automatic artefact rejection system removed signals contaminated by large eye movements and blinks.

All stimuli were calibrated using an ILT 1700 radiometer with SED033/Y/R luminance detector (Able Instruments and Controls, Reading, UK) assuming a 7-mm pupil with no correction for the Stiles-Crawford effect. The wavelengths of the light sources were measured using a spectroradiometer (1201 Specbos; Horiba Jobin Yvon Ltd, Middlesex, UK).

Long-Duration ERGs

Focal long duration ERGs of increasing stimulus sizes were recorded using a red circular stimulus (peak wavelength 660 nm, 250 ms, 55 cd/m^2, 2 Hz) on a rod saturating blue background (peak wavelength 469 nm, 100 scot cd/m^2). The stimulus and background luminance were chosen to minimize stray light effects in focal ERG recordings as proposed in an earlier study by Kondo et al.[14] Focal stimulation was produced by mounting the miniature Ganzfeld LED tube in the middle of a light box (44 × 44 × 10 cm) to produce a circular stimulus (Fig. 1A). The light box contained a strip of white LEDs (color temperature >7000 K) passed through a blue filter (Lee Filter 068 Sky Blue, Lee Filters, Hampshire, UK), which produced a rod desensitizing blue surround (peak wavelength 454 nm, 140 scot cd/m^2). The angular diameters of the focal stimuli were 5.5°, 10°, 15°, 20°, 30°, 45°, and 60°; they were obtained by varying the viewing distance (VD; Fig. 1A, Table 1). The focal stimuli were centered on the fovea by asking the participant to fixate the intersection of a pair of cross-hairs centered in the middle of the stimulus. Head movements were restrained with a headrest. A full-field (110°) ERG was recorded by holding the miniature Ganzfeld directly to the eye (Fig. 1B). The dimensions of the circular stimuli are shown in Table 1.

Brief-Flash ERGs

Focal brief-flash ERGs were recorded using the same setup used for the long-duration ERGs, except that the duration was decreased to 5 ms, the stimulus temporal frequency was increased to 4 Hz, and the luminance was set to 0.28 cd.s/m^2 to match the long flash stimulus luminance. The angular diameters of the stimuli were 5°, 10°, 15°, 20°, 30°, 60° and full field (110°; Table 1).

Signal Analysis

Electroretinograms were Fourier analyzed to remove high frequency signals above 50 Hz. The amplitudes of the a- and b-wave were measured as recommended by the International Society of Clinical Electrophysiology of Vision (ISCEV).[15] The PhNR-ON (PhNR in brief-flash ERG) amplitude was measured from the peak of the b-wave to the trough of the PhNR. The d-wave amplitude was measured from light offset to the first positive peak after light offset. The PhNR-OFF was measured from the d-wave peak to the PhNR-OFF trough. An additional positive potential was observed immediately following stimulus offset in ERGs produced by stimuli larger than 30° (arrowed in Fig. 2). In these cases, the PhNR-OFF was measured from the second positive peak since its time-to-peak corresponded to the d-wave in the smaller stimulus ERGs.

Downloaded from arvojournals.org on 05/13/2019

Investigative Ophthalmology & Visual Science

Table 1. Dimensions of the Stimulus Sizes Used in the Study and the Estimated Number of RGCf and Cones Contained in Their Areas

Stimulus Diameter, deg (VD, cm)	Surround Background Dimension, deg	Annulus Dimension, deg (Eccentricity, deg)	Stimulus Area, deg^2 (Annulus Area, deg^2)	Total RGCf in Annulus	ON-RGCf in Annulus Area	OFF-RGCf in Annulus Area	Total RGCf Density, RGCf/deg^2	ON-RGCf Density	OFF-RGCf Density	Cones in Annulus	Average Cone Density (cells/deg^2)
5 (66.4)	37 × 37	0–5 (1.3)	19.6 (19.6)	123,728	-	-	7212	-	-	75,530	3500
5.5 (60.4)	**40 × 40**	**0–5.5 (1.4)**	**23.8 (23.8)**	**136,063**	**67,351**	**68,712**	**6491**	**3214**	**3278**	**88,057**	**3073**
10 (33.2)	67 × 67	5–10 (3.8)	78.5 (58.9)	110,293	-	-	1857	-	-	126,152	1380
		5.5–10 (3.9)	**78.5 (54.8)**	**97,959**	**48,293**	**49,665**	**1779**	**877**	**902**	**113,986**	**1255**
15 (22.0)	**90 × 90**	10–15 (6.3)	176.7 (98.2)	90,485	**43,876**	**46,609**	917	**445**	**473**	129,287	837
20 (16.5)	106 × 106	15–20 (8.8)	314.2 (137.4)	78,977	37,213	41,764	573	270	303	132,062	690
30 (10.8)	128 × 128	20–30 (12.5)	668.4 (354.2)	98,368	44,784	53,620	224	102	123	272,448	542
45 (7.0)	145 × 145	**30–45 (18.8)**	**1551.9 (883.6)**	138,451	**59,517**	**79,024**	**187**	**81**	**107**	**429,482**	**433**
60 (5.0)	**154 × 154**	30–60 (22.5)	2788.95 (2120.6)	271,687	-	-	139	-	-	883,937	387
		45–60 (26.3)	**2788.9 (1237.0)**	**133,146**	**55,078**	**78,067**	**107**	**44**	**63**	**454,455**	**359**
110 (held to eye)	NA	60–110 (42.5)	9464.8 (6675.9)	291,263	**122,800**	**168,462**	43	**18**	**25**	1,695,208	257

Values in bold apply to long duration stimulus only. The estimated figures for RGCfs and cones were calculated from data and formula provided by references 12, and 14 through 16. Details are provided in the Methods section. NB, the area of the optic nerve head (38.48 deg^2; assuming a diameter of 7° and beginning at 11° from the fovea[13]) has been subtracted from angular areas of stimuli >30°.

Table 2. The Values of Constants for Equation 1 in Four Meridians[13]

Meridian, k*	a	r_2	r_e
Temporal	0.99	1.06	22.14
Superior	0.99	1.04	16.35
Nasal	0.98	1.08	7.63
Inferior	1.00	0.99	12.13

* Meridians refer to visual field locations.

The group-averaged ERGs for each stimulus size were normalized to their respective b-wave amplitudes to facilitate waveform comparison. The amplitude and time-to-peak of ERG components for each stimulus size were plotted as a function of stimulus area. Response density profiles were obtained for the PhNR components and compared to density profiles of RGCs and cones. To obtain the response density of the ERG components, the arithmetic difference in amplitude between two successive stimulus sizes (annulus amplitude) was divided by the area of the annulus and the quotient plotted as a function of the midpoint (in degrees) of the annulus. Calculations for RGCf and cones were derived from published data and are described in the section below.

Calculation of RGCf and Cone Densities

A formula by Watson[13] was used to calculate RGCf field density (RGCf/deg^2) as a function of eccentricity in the human retina:

$$d_{gf}(r,k) = d_{gf}(0) * \left[a_k \left(1 + \frac{r}{r_{2,k}}\right)^{-2} + (1 - a_k) exp\left(\frac{-r}{r_{e,k}}\right)\right] \quad (1)$$

where d_{gf} (r, k) is the density of RGCfs at eccentricity, r, in degrees along meridian, k; $d_{gf}(0)$ is the density of receptive fields at the center of the fovea (33,163.2 RGCf/deg^2), a_k is the weighting function of the first term, r_2 is the eccentricity at which RGC receptive field density is reduced by a factor of 4 (and spacing is doubled), and r_e is the meridian dependent scale factor. The values of the constants are provided in Table 2.

The formula provides RGCf densities for each of four meridians. However, since a circular stimulus centered on the fovea was used in this study, the mean density of the four meridians was calculated and used instead. The area of the blind spot (38.5 deg^2) was subtracted from the areas covered by stimuli >30°. The mean cumulative counts of RGCf as a function of eccentricity, were calculated by integrating the mean density at eccentricity, r, (using the trapezoid rule) and multiplying this by $2\pi r$ to account for the increasing circumference.[13]

Computations regarding the midget RGCs (mRGC) were based on the published results of Dacey[16] and Drasdo.[17] Calculations for ON and OFF mRGCs were based on the ratio of ON to OFF mRGCs from 0° to 5° = 1:1; from 5° to 25° = 1:1 to 1:1.69; and beyond 25° = 1:1.69.[17] Of the total RGCs in the human retina, parasol RGCs (pRGCs) constitute about 5% at the fovea and progressively increases to 20% in the periphery.[18] The ON:OFF ratio of pRGCs was then computed to be 0.4:0.6 based on the dendritic field size differences between ON and OFF pRGCs.[19] The proportion of other types of RGCs was calculated by subtracting the sum of the midget and parasol RGCs from the total number of RGCs at each eccentricity. The ON to OFF ratio for the other RGC types was assumed to be 1:1.

The dimensions of the circular stimuli, the annuli, their midpoints (eccentricity) and estimated RGCf and cone counts are shown in Table 1.

Downloaded from arvojournals.org on 05/13/2019

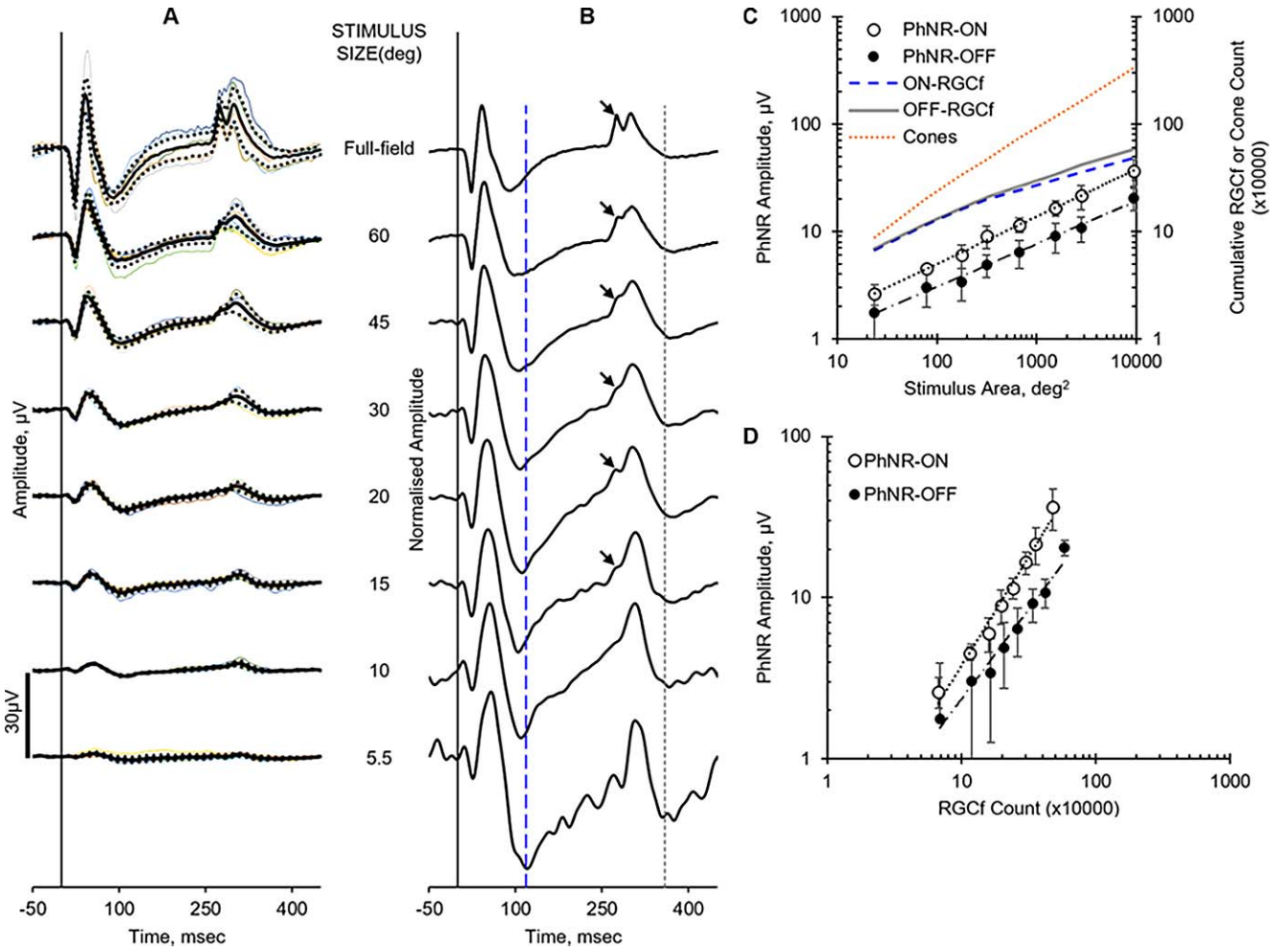

Figure 2. (**A**) Group-averaged long duration ERGs (*thick black lines*) recorded from six participants (*thin colored lines*) in response to increasing stimulus size (*bottom* to *top*). *Dotted lines* represent 95% CI. (**B**) The same group-averaged ERGs for each stimulus size which have been normalized to their respective b-wave amplitudes. *Arrows* indicate an emerging additional positive peak on the rising phase of the d-wave. The *blue long dashes* and *gray short dashes* mark the group-averaged time-to-peak of the PhNR-ON (118.38 ms) and the PhNR-OFF (359.25 ms) respectively of the 5.5° stimulus. (**C**) Relationship between mean PhNR-ON and -OFF amplitudes of the long duration ERG and stimulus area. The equation of the line passing through the PhNR-ON data (*open circles*) is $y = 0.65x^{0.44}$, $R^2 = 1.00$, while that for the PhNR-OFF (*black dots*) is $y = 0.49x^{0.40}$, $R^2 = 0.99$. Cumulative counts of ON-RGCf (*blue dashes*), OFF-RGCf (*gray line*), and cones (*orange dotted line*) plotted from the data provided by Watson[13] are shown for comparison. (**D**) Relationship between mean amplitudes of PhNR-ON and –OFF, and estimated number of ON- and OFF-RGCf in increasing stimulus area. The equation of the line passing through the PhNR-ON data is $y = 7{*}10^{-7}x^{1.35}$, $R^2 = 0.98$; PHNR-OFF: $y = 6{*}10^{-6}x^{1.11}$, $R^2 = 0.97$. *Error bars* represent 95% CI.

Statistical Analysis

Regression analysis was used to determine the following relationships: PhNR amplitude and stimulus area, PhNR amplitude and calculated RGCfs, PhNR density and the RGCf density, and response per RGCf as a function of retinal eccentricity. The relationships were determined by finding the regression line with the highest R^2 value using spreadsheet software (Excel 2016; Microsoft Corp., Redmond, WA, USA). As the sample size was less than 30, 95% confidence intervals were calculated using the Student's *t*-distribution.

Results

Participants

For the long-duration ERGs, six participants (67% female; age range 25–37 years, mean 29.33 ± 4.23 years SD), were recruited. For the brief-flash ERGs, 12 participants (58% female; age range 22 to 31 years, mean age 27.30 + 2.67 years SD) were recruited. Two participants from the long-duration study took part in the brief-flash study.

Long-Duration ERGs

The traces from individual participants ($n = 6$) are shown in Figure 2A. The group-averaged traces (Fig. 2A) and the mean amplitudes of the PhNR (Fig. 2C) demonstrated an increase with the stimulus size. The data was best fit by a straight line on a log-log plot, suggesting that the underlying relationship was a power law function (PhNR-ON: $y = 0.66x^{0.44}$, $R^2 = 1.00$; PhNR-OFF: $y = 0.49x^{0.40}$, $R^2 = 0.99$; Fig. 2C). A similar relationship was found between the PhNR-ON amplitude and the calculated number of ON-RGCf stimulated ($y = 7{*}10^{-7}x^{1.345}$, $R^2 = 0.98$) as well as between the PhNR-OFF amplitude and the calculated OFF-RGCf stimulated ($y = 6{*}10^{-6}x^{1.11}$, $R^2 = 0.97$) in Figure 2D. The mean time-to-peak

Investigative Ophthalmology & Visual Science

Downloaded from arvojournals.org on 05/13/2019

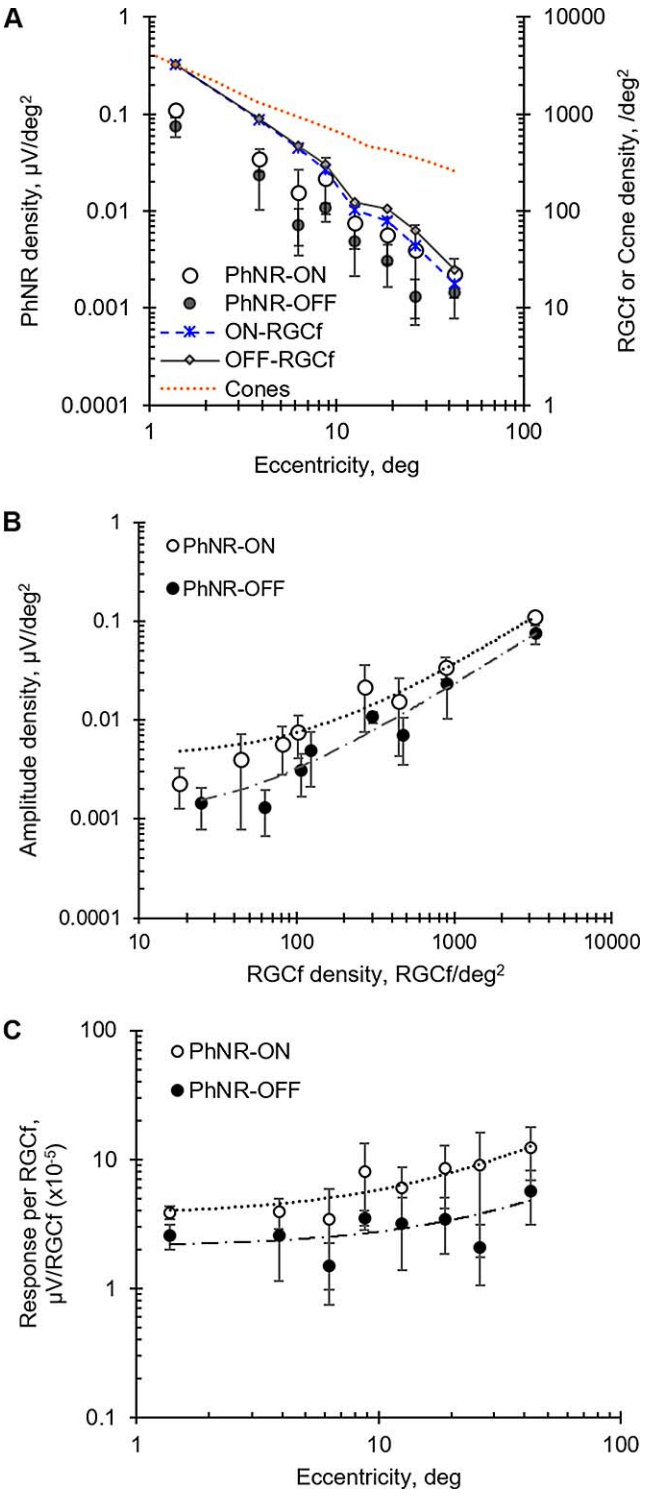

FIGURE 3. (**A**) Amplitude densities of the PhNR-ON and PhNR-OFF components as a function of eccentricity. ON-RGCf (*blue dashes*), OFF-RGCf (*gray line*), and cone (*orange dotted line*) densities plotted from the data provided by Watson[13] are shown for comparison. (**B**) Relationship between PhNR density and RGCf density. The equation for the PhNR-ON line is $y = 3^{*}10^{-5}x + 0.0043$; $R^2 = 0.99$. The equation for the PhNR-OFF line is $y = 2^{*}10^{-5}x + 0.0011$; $R^2 = 0.99$. (**C**) Estimated PhNR-ON and PhNR-OFF amplitude contributed by each ON-RGC and OFF-RGC respectively as a function of eccentricity. The equation of the PhNR-ON line is $y = 0.21x + 3.74$; $R^2 = 0.85$. The equation of the PhNR-OFF line is $y = 0.06x + 2.12$; $R^2 = 0.49$. *Error bars* represent 95% CI.

of the PhNR-ON showed a significant decrease with increasing stimulus area (F [1, 6] = 15.44, $P = 0.0077$), however, PhNR-OFF time-to-peak did not show any significant pattern (F [1, 6] = 3.04, $P = 0.1320$).

The waveforms of the normalized ERGs in response to the smaller stimulus sizes (5.5°–30°) were different from those in response to the larger sizes (45°, full-field; Fig. 2B). The amplitude of the PhNR-ON and PhNR-OFF components in comparison to the b- and d-waves was greater in the ERGs of the smaller stimulus sizes than in the larger stimulus sizes. A ledge on the rising limb of the d-wave (arrowed), first seen on the 15° ERGs, became progressively more prominent and developed into a separate peak in the 60° and full-field ERGs.

The response density plot in Figure 3A, showed that both PhNR-ON and PhNR-OFF densities were maximal at the fovea and decreased toward the periphery. The density plots of the PhNR-ON and PhNR-OFF were qualitatively similar to those of the ON (blue dashed line) and OFF (gray-dashed lines) RGCf densities. A cone density plot derived from the data provided by Curcio et al.[20] is also shown as a dashed orange line in Figure 3A. It may be seen that although cone density dropped with eccentricity, its profile, unlike that of the RCGfs, deviated from that of the PhNR data from an eccentricity of about 4°.

Regression analysis showed that the highest R^2 value obtained for the relationship between the PhNR-ON density and ON-RGCf density was given by a linear function ($y = 3^{*}10^{-5}x + 0.0043$, $R^2 = 0.99$), as was the relationship between the PhNR-OFF density and OFF-RGCf density ($y = 2^{*}10^{-5}x + 0.0011$, $R^2 = 0.99$; Fig. 3B). Both relationships were highly significant (PhNR-ON: T = 43.8, P value < 0.0001; PhNR-OFF: $T = 49.5$; $P < 0.0001$). The response per RGC (response in annulus/number of RGCf in annulus) of the PhNR-ON and PhNR-OFF both showed a significant increase with eccentricity and were best fit by a linear function (PhNR-ON: $y = 0.21x + 3.74$; $R^2 = 0.85$; PhNR-OFF: $y = 0.06x + 2.12$, $R^2 = 0.49$; Fig. 3C).

Brief-Flash ERGs

The amplitude of the PhNR increased with stimulus area (Fig. 4A) and as observed in the long-duration ERG, the ratio of the PhNR amplitude to the b-wave amplitude reduced as stimulus area increased (Fig. 4B). PhNR time-to-peak decreased but not significantly with increasing stimulus area (F [1, 6] = 1.46, $P = 0.28$; Fig. 4B). The relationship between the amplitude of the PhNR and the stimulus area was best described by a power regression line ($y = 0.55x^{0.49}$, $R^2 = 1.00$) (Fig. 4C), as found for the long-duration stimulus. A similar relationship was found between the brief PhNR amplitude and the estimated number of RGCfs ($y = 5^{*}10^{-5}x^{-7.75}$, $R^2 = 0.96$, $P < 0.0001$). The waveforms of the normalized brief flash ERGs were similar for all stimulus sizes except for the full-field, which had a positive going component interrupting the descending limb of the b-wave (the i-wave, arrowed) (Figure 4B).

The brief-flash PhNR density was maximal at the fovea and declined rapidly toward the periphery in a way similar to Watson's RGCf density data (Fig. 5A). As seen for the long-duration stimulus, the relationship between the PhNR density and the RGCf density was best described by a linear function ($y = 2^{*}10^{-5}x + 0.0059$, $R^2 = 1.00$; Fig. 5B). Once again, the cone density profile showed poor overlap with the PhNR density profile (Fig. 5A). The calculated response per RGC increased with eccentricity as previously observed for the long-duration PhNRs (Fig. 5C).

Investigative Ophthalmology & Visual Science

Downloaded from arvojournals.org on 05/13/2019

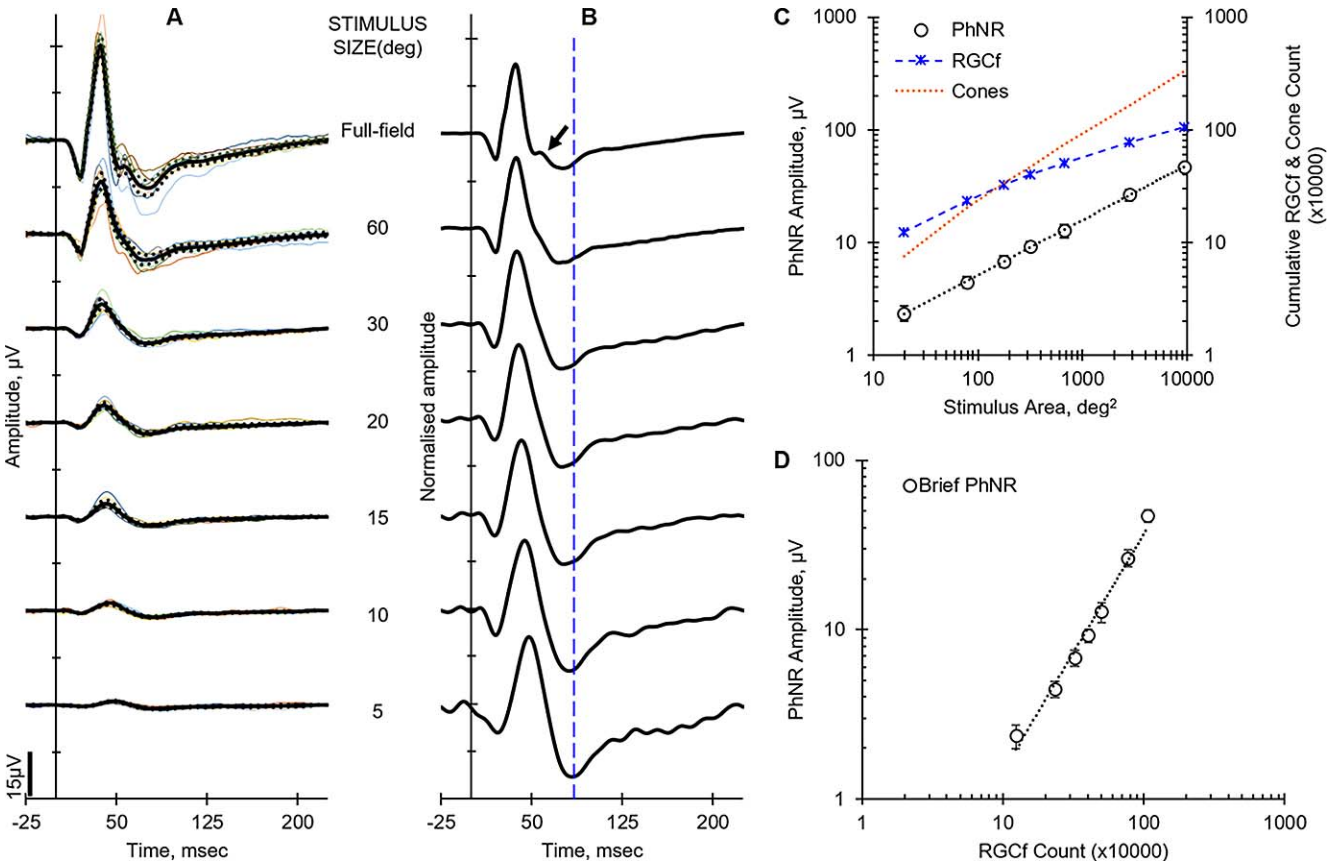

Figure 4. (**A**) Group-averaged brief-flash ERGs (*thick black lines*) recorded from 12 participants (*thin colored lines*) in response to increasing stimulus size (*bottom* to *top*). *Dotted lines* show the 95% CI. (**B**) The same group-averaged ERGs for each stimulus size that have been normalized to their respective b-wave amplitudes. *Arrow* indicates the positive wavelet (i-wave) on the falling phase of the b-wave. The *blue dashed line* marks the group averaged time-to-peak of the PhNR (84.64 ms) of the 5° stimulus. (**C**) Relationship between mean amplitudes of the brief flash PhNR and stimulus area fitted by a power regression line ($y = 0.55x^{0.49}$, $R^2 = 1.00$). Cumulative counts of RGCf (*blue dashes*) and cones (*orange dotted line*) plotted from the data provided by Watson[13] are shown for comparison. (**D**) Relationship between mean amplitudes of the brief PhNR and estimated number of RGCfs in increasing stimulus areas. Regression line is $y = 1^{*}10^{-7}x^{1.40}$, $R^2 = 0.98$. *Error bars* represent 95% CI.

Discussion

Effect of Stimulus Size on PhNR Amplitude and ERG Waveform

The amplitude of the PhNR increased with increasing stimulus area. This was attributed to the increasing cumulative number of cells stimulated[20–22] (see also Table 1) and agrees with previous studies that have reported an increase in the amplitudes of other ERG components with stimulus size.[23–27] However, the magnitude of the increase was not uniform across ERG components.[23,28] For example, in Figure 2B, as stimulus area increased, the b-wave amplitude, a response dominated by bipolar cell activity,[29] increased with respect to the PhNR amplitude. These changes in ERG waveform are attributable to a change in the relative proportions of the different types of retinal cells with increasing eccentricity.[17,20,22,30–32]

In the long-duration ERGs, the emergence of two distinct positive peaks after stimulus offset in the 60° and full-field ERGs, not seen in the ERGs produced by smaller stimuli, was notable. These peaks are often seen in full-field long duration ERGs.[1,29,33–35] Pharmacologic evidence attributes the first positive peak, often designated as the d-wave, to the depolarization of OFF-bipolar cells after stimulus offset while the second positive peak is attributed to depolarization of cones after stimulus offset.[29,34] The timing of the d-wave (single peak after stimulus offset) of the smaller stimuli (5.5°–45°) more closely matched the timing of the second peak in the larger stimuli (60° and full-field), suggesting that the cellular origins of the focal d-wave and those of the full-field d-wave (i.e., the first peak) may not be the same.

It was further observed that the times-to-peak of the PhNR-ON decreased significantly with increasing stimulus sizes (Fig. 2B). A similar but not significant decrease was observed for the brief flash PhNR. The decrease may be related to the reported increase in conduction velocity of RGC axons with increasing eccentricity[36] and/or the presence of Henle fibers in the central 30° field of the retina, which increase toward the foveola.[17]

Relationship Between PhNR Amplitude and RGC Population

This study has determined the relationship between the PhNR amplitude and RGC population by mapping the amplitudes of the PhNR to the estimated numbers of RGCfs within a given area. Although qualitative similarities between the profiles of both the PhNR amplitude and RGCf numbers with stimulus size were observed, the precise characteristics of the slopes were clearly distinct (see Fig. 2C). This suggested that the increase in amplitude was not entirely due to increasing RGC numbers. To better understand the relationship, the cumulative PhNR and RGCf data were reanalyzed to derive densities

Downloaded from arvojournals.org on 05/13/2019

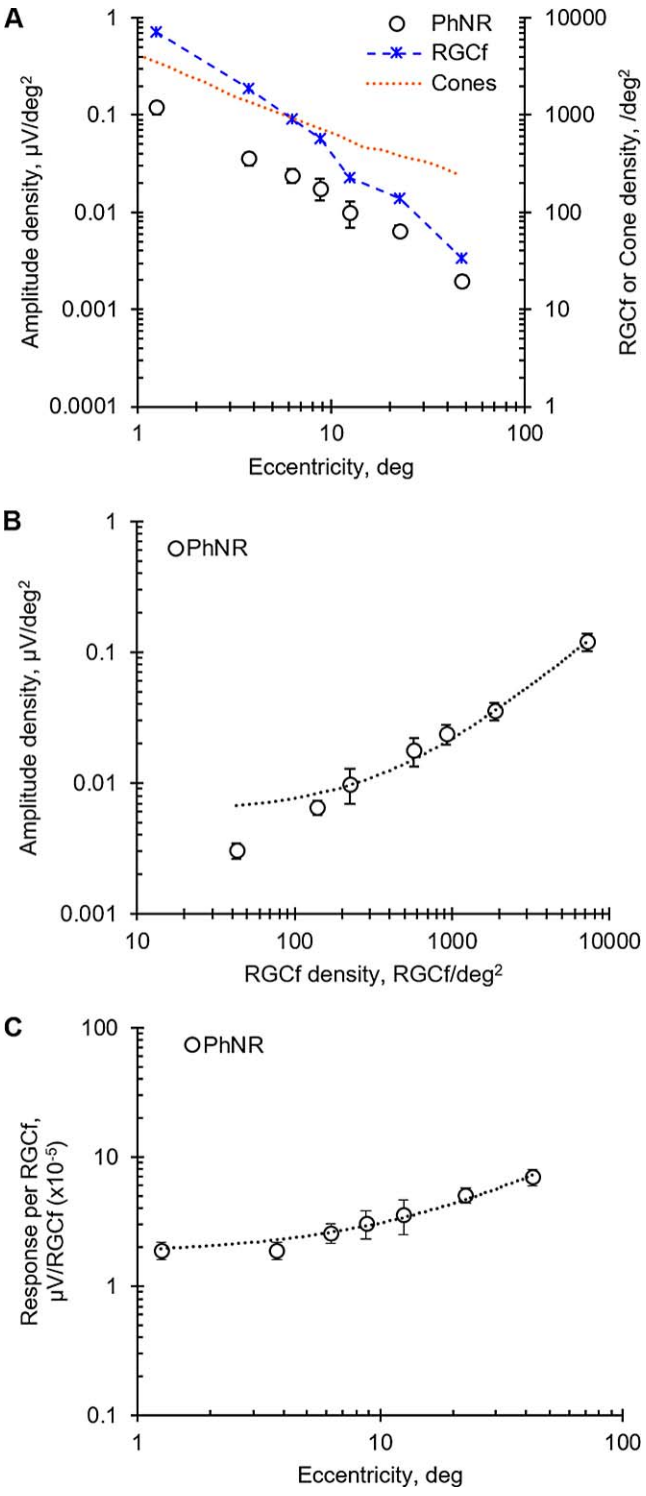

FIGURE 5. (**A**) Amplitude density of the brief flash PhNR plotted as a function of eccentricity. RGCf density (*blue dashes*) and cone density (*orange dotted line*) plotted from the data provided by Watson[13] are shown for comparison. (**B**) Relationship between the brief PhNR density and RGCf density fitted by linear regression line ($y = 2*10^{-5}x + 0.0059$, $R^2 = 1.00$). (**C**) Estimated PhNR amplitude contributed by each RGC as a function of eccentricity. The equation of the regression line (*dotted line*) is given by $y = 0.13x + 1.81$, $R^2 = 0.98$. *Error bars* represent 95% CI.

(i.e., PhNR amplitude and RGCf numbers per unit area). The density data shown in Figure 3A and Figure 5A, described on log-log axes for consistency, describe a linear relationship with both variables declining monotonically with increasing eccentricity. As might be expected on the basis of pharmacologic studies that have shown the PhNR to be dominated by responses from retinal ganglion cells,[1] the electrophysiologic relationship with this component of the ERG and RCG cell density was strong ($R^2 > 0.98$).

Finally, this study estimated PhNR amplitude per RGC (see Figs. 3C, 5C). This analysis suggested that the response produced by a single RGC increased with eccentricity. In the long-duration ERG, the ON-RGC response (PhNR-ON) showed about a 3-fold increase from approximately $4*10^{-5}$ µV per cell at the fovea to $12*10^{-5}$ uV per cell in the periphery, while the OFF-RGC response (PhNR-OFF) per cell for the PhNR-OFF showed a 2-fold increase from approximately $3*10^{-5}$ µV per cell to $6*10^{-5}$ µV per cell. The brief PhNR showed about a 3-fold increase from $2*10^{-5}$ µV to $7*10^{-5}$ µV. When the data was reanalyzed using PhNR amplitude measured from baseline to trough (BT), the pattern was similar (see Supplementary Material Fig. S1). Specifically, the PhNR-ON increased about three times from $2*10^{-5}$ µV per cell at the fovea to $7*10^{-5}$ µV per cell in the peripheral retina; while PhNR-OFF increased from $1*10^{-5}$ µV per cell to $3*10^{-5}$ µV per cell. The brief PhNR (BT) per cell showed a 2-fold increase from about $1*10^{-5}$ µV to $2*10^{-5}$ µV/RGCf.

The increase in response per cell with eccentricity, may be related to the increase in the dendritic field and/or cell size of the RGCs with eccentricity.[16,19,37–40] For the range of eccentricities examined in this study (i.e., 1°–45° ~ 0.3–12 mm), morphometric data from previous studies showed that the soma sizes of midget and parasol ganglion cells each increase approximately by a factor of 2.[37,38] Dendritic field diameter, on the other hand, increases about 20- to 40-fold for midget ganglion cells and 10-fold for parasol ganglion cells.[16,19,37,38] The increase in PhNR amplitude per RGC with eccentricity therefore appears to be more closely related to soma size than to dendritic field size. Secondly, since the PhNR is also related to spiking activity in RGC axons,[1] it is also possible that the longer axon length of more peripheral RGCs may account for the increasing responses. Specifically, that as action potentials have to travel a longer distance to reach the disc, more extracellular potassium and consequently a larger PhNR amplitude may be produced.

Another possible explanation for the observed increase in the response per cell with eccentricity is related to the cellular generators of the PhNR. Although the RGCs are considered as the primary generators of the PhNR, there is evidence to show that the photoreceptors, amacrine cells, Müller, and other glial cells also contribute.[1,4,5,41,42] Due to the relative increase in the numbers of these cells to the RGCs toward the retinal periphery,[20,22,32] the increase in PhNR amplitude may be due, for example, to increased contributions from glial K^+ currents, known to contribute to the PhNR[4] and not strictly to RGC density or numbers.

Limitations of the Study

This study based its calculations on a model of RGC distribution reported by one study.[13] The observation that the amplitude per RGC increases with eccentricity assumes that the model for RGCf density is correct. Watson's model was carefully derived from data made available by Curcio and colleagues (available at https://jov.arvojournals.org/data/journals/jov/933548/jov-03833-2013-s01.txt. Accessed 12/12/2018) and used in the seminal publications about the distribution of photoreceptors[20] and RGCs[17,22] in the human

Investigative Ophthalmology & Visual Science

Downloaded from arvojournals.org on 05/13/2019

retina. Although there are good reasons to believe that Watson's model is accurate, the conclusion that RGC output per cell increases with eccentricity is only as good as the underlying model.

In addition, wide interindividual variations in RGC numbers exist in the normal population.[22] Based on the standard deviation (0.4 million) reported for mean (1.07 million) RGC numbers in the human retina,[22] it was estimated that the 95% confidence interval around the values reported here could vary by up to 30%. Furthermore, the low number of participants used in this study precluded investigations into any age- or sex-dependent differences in the results. Since the stimulus area for the focal ERG was determined by adjusting the viewing distance, stimulus area was susceptible to variations in eye or head position. If up to 1 cm variation in the viewing distance due to variations in position of the eye in the orbit is assumed, the margin of error associated with the stimulus size varies from 3% for the 5° to 27% for the 60° stimulus. The monocular visual field is roughly an ellipse (130° high by 160° wide). However, the handheld Ganzfeld stimulator had a flat, circular surface which prevented complete coverage the eye socket. We estimate that only 110° of the visual field was covered by the stimulator when it was held close to the eye. Although the unstimulated retinal area was large, it contained less than 10% of the entire RGC population and thus the error associated with our estimate of the visual field stimulated was expected to be small.

Another limitation of this study was that it did not account for the normal variations in the optic nerve head size (diameters range from 5°–8°).[43] However, the overall effect of this is negligible since it mainly affected calculations involving the 30° stimulus and did not introduce an error of more than 1% in the overall results.

Finally, although we sought to minimize any stray light effects by adopting a stimulus and background configuration that has previously be shown to avoid stray light effects in rhesus monkeys,[14] we cannot rule out the possibility that stray light might have contributed to the signal measured. Specifically, the background was only full-field for the 110° stimulus, and was progressively smaller for reducing stimulus sizes (Table 1). If scattered light was, indeed, contributing to the magnitude of the PhNR, we might expect to record a relatively large response for the smaller stimuli (where the background was of a smaller angular subtense). In fact, the opposite effect was seen in this study, where the response per RGC was greatest for the peripheral retina assessed using the largest stimuli. On this basis, it seems unlikely that scattered light can explain our observation that the response per RGC increases with eccentricity.

Clinical Implications

The PhNR is a widely used protocol for assessing RGC and inner retinal function,[15] and was recently covered by ISCEV standards.[44] This study suggests that a loss in PhNR amplitude would depend on both the size and the location of the lesion, with peripheral lesions having a relatively greater impact than more central ones. This may explain the observation in other studies[9,10,45] that the full-field ERG is less sensitive to central lesions than peripheral ones. As such, the locus of the disease would have to be considered in any future standard for recording the PhNR.

Conclusions

This study demonstrated that the PhNR-ON and PhNR-OFF components of the long-duration ERG, as well as the PhNR of the brief-flash ERG, increased in amplitude with increasing stimulus area. This was qualitatively similar to increases in the estimated cumulative RGCf counts in the stimulated areas. However, the changes in PhNR amplitude with increasing stimulus area were not entirely explained by increasing RGC count. The contribution of a single RGC to the PhNR amplitude appeared to depend on its eccentricity with peripheral units producing a signal 2 to 3 times greater than central ones. Therefore, a specific reduction in PhNR amplitude may not be directly related to the number of RGCs lost, the location of the loss is an important variable. Finally this study showed that the focal d-wave and the full-field d-wave (first peak after stimulus offset) did not have similar implicit times suggesting that the origins of these components may not be the same.

Acknowledgments

Supported by the Ghana Education Trust Fund (EKAM).

Disclosure: **E.K.A. Morny**, None; **K. Patel**, None; **M. Votruba**, None; **A.M. Binns**, None; **T.H. Margrain**, None

References

1. Viswanathan S, Frishman LJ, Robson JG, Harwerth RS, Smith EL, Smith EL III. The photopic negative response of the macaque electroretinogram: reduction by experimental glaucoma. *Invest Ophthalmol Vis Sci*. 1999;40:1124–1136.
2. Viswanathan S, Frishman LJ, Robson JG. The uniform field and pattern ERG in macaques with experimental glaucoma: removal of spiking activity. *Invest Ophthalmol Vis Sci*. 2000;41:2797–2810.
3. Rangaswamy NV, Shirato S, Kaneko M, Digby BI, Robson JG, Frishman LJ. Effects of spectral characteristics of Ganzfeld stimuli on the photopic negative response (PhNR) of the ERG. *Invest Ophthalmol Vis Sci*. 2007;48:4818–4828.
4. Thompson DA, Feather S, Stanescu HC, et al. Altered electroretinograms in patients with KCNJ10 mutations and EAST syndrome. *J Physiol*. 2011;589:1681–1689.
5. Luo X, Frishman LJ. Retinal pathway origins of the pattern electroretinogram (PERG). *Invest Ophthalmol Vis Sci*. 2011; 52:8571–8584.
6. Nakamura H, Hangai M, Mori S, Hirose F, Yoshimura N. Hemispherical focal macular photopic negative response and macular inner retinal thickness in open-angle glaucoma. *Am J Ophthalmol*. 2011;151:494–506.
7. Shen X, Huang L, Fan N, He J. Relationship among photopic negative response, retinal nerve fiber layer thickness, and visual field between normal and POAG eyes. *ISRN Ophthalmol*. 2013;2013:182021.
8. Tamada K, Machida S, Oikawa T, Miyamoto H, Nishimura T, Kurosaka D. Correlation between photopic negative response of focal electroretinograms and local loss of retinal neurons in glaucoma. *Curr Eye Res*. 2010;35:155–164.
9. Tamada K, Machida S, Yokoyama D, Kurosaka D. Photopic negative response of full-field and focal macular electroretinograms in patients with optic nerve atrophy. *Jpn J Ophthalmol*. 2009;53:608–614.
10. Machida S, Tamada K, Oikawa T, et al. Comparison of photopic negative response of full-field and focal electroretinograms in detecting glaucomatous eyes. *J Ophthalmol*. 2011;2011:564131.
11. Moss HE, Park JC, McAnany JJ. The photopic negative response in idiopathic intracranial hypertension. *Invest Opthalmology Vis Sci*. 2015;56:3709–3714.
12. Machida S. Clinical applications of the photopic negative response to optic nerve and retinal diseases. *J Ophthalmol*. 2012;2012:397178.

Investigative Ophthalmology & Visual Science

Downloaded from arvojournals.org on 05/13/2019

13. Watson AB. A formula for human retinal ganglion cell receptive field density as a function of visual field location. *J Vis*. 2014;14(7):15.
14. Kondo M, Kurimoto Y, Sakai T, et al. Recording focal macular photopic negative response (PhNR) from monkeys. *Invest Ophthalmol Vis Sci*. 2008;49:3544–3550.
15. McCulloch DL, Marmor MF, Brigell MG, et al. ISCEV Standard for full-field clinical electroretinography (2015 update). *Doc Ophthalmol*. 2015;130:1–12.
16. Dacey DM. The mosaic of midget ganglion cells in the human retina. *J Neurosci*. 1993;13:5334–5355.
17. Drasdo N, Millican CL, Katholi CR, Curcio CA. The length of Henle fibers in the human retina and a model of ganglion receptive field density in the visual field. *Vis Res*. 2007;47: 2901–2911.
18. Dacey DM. Physiology, morphology and spatial densities of identified ganglion cell types in primate retina. *Ciba Found Symp*. 1994;184:12–28; discussion 28–34, 63–70.
19. Dacey DM, Petersen MR. Dendritic field size and morphology of midget and parasol ganglion-cells of the human retina. *Proc Natl Acad Sci U S A*. 1992;89:9666–9670.
20. Curcio CA, Sloan KR, Kalina RE, Hendrickson AE. Human photoreceptor topography. *J Comp Neurol*. 1990;292:497–523.
21. Osterberg G. Topography of the layer of rods and cones in the human retina. *Acta Ophthalmol Suppl*. 1935;6:1–103.
22. Curcio CA, Allen KA. Topography of ganglion cells in human retina. *J Comp Neurol*. 1990;300:5–25.
23. Errico P, Falsini B, Porciatti V, Cefala FM. The human focal electroretinogram as a function of stimulus area. *Doc Ophthalmol*. 1990;75:41–48.
24. Junghardt A, Wildberger H, Robert Y, Torok B. Pattern electroretinogram and visual evoked potential amplitudes are influenced by different stimulus field sizes and scotomata. *Doc Ophthalmol*. 1993;83:139–149.
25. Murray IJ, Parry NR, Kremers J, Stepien M, Schild A. Photoreceptor topography and cone-specific electroretinograms. *Vis Neurosci*. 2004;21:231–235.
26. Jacob MM, Pangeni G, Gomes BD, et al. The spatial properties of L- and M-cone inputs to electroretinograms that reflect different types of post-receptoral processing. *PLoS One*. 2015; 10:e0121218.
27. Seiple W, Greenstein V, Holopigian K, Carr R. Changes in the focal electroretinogram with retinal eccentricity. *Doc Ophthalmol*. 1988;70:29–36.
28. Brindley BGS, Westheimer G. The spatial properties of the human electroretinogram. *J Physiol*. 1965:518–537.
29. Sieving PA, Murayama K, Naarendorp F. Push-pull model of the primate photopic electroretinogram: a role for hyperpolarizing neurons in shaping the b-wave. *Vis Neurosci*. 1994; 11:519–532.
30. Kolb H. How the retina works. *Am Sci*. 2003;91:28–35.
31. Kolb H. Simple anatomy of the retina. In: Kolb H, Nelson R, Fernandez E, Jones B, eds. *Webvision: The Organisation of the Retina and Visual System*. Salt Lake City; 2011.
32. Martin PR, Grünert U. Spatial density and immunoreactivity of bipolar cells in the macaque monkey retina. *J Comp Neurol*. 1992;323:269–287.
33. Sustar M, Cvenkel B, Brecelj J. The effect of broadband and monochromatic stimuli on the photopic negative response of the electroretinogram in normal subjects and in open-angle glaucoma patients. *Doc Ophthalmol*. 2009;118:167–177.
34. Ueno S, Kondo M, Ueno M, Miyata K, Terasaki H, Miyake Y. Contribution of retinal neurons to d-wave of primate photopic electroretinograms. *Vision Res*. 2006;46:658–664.
35. Horn FK, Gottschalk K, Mardin CY, Pangeni G, Junemann AG, Kremers J. On and off responses of the photopic fullfield ERG in normal subjects and glaucoma patients. *Doc Ophthalmol*. 2011;122:53–62.
36. Stanford LR. Conduction velocity variations minimize conduction time differences among retinal ganglion cell axons. *Science*. 1987;238:358–360.
37. Rodieck R, Binmoeller K, Dineen J. Parasol and midget ganglion cells of the human retina. *J Comp Neurol*. 1985;233: 115–132.
38. Watanabe M, Rodieck RW. Parasol and midget ganglion cells of the primate retina. *J Comp Neurol*. 1989;289:434–454.
39. Silveira LCL, Perry VH. The topography of magnocellular projecting ganglion cells (M-ganglion cells) in the primate retina. *Neuroscience*. 1991;40:217–237.
40. Yamada ES, Silveira LC, Perry VH. Morphology, dendritic field size, somal size, density, and coverage of M and P retinal ganglion cells of dichromatic Cebus monkeys. *Vis Neurosci*. 1996;13:1011–1029.
41. Bush RA, Sieving PA. A proximal retinal component in the primate photopic ERG a-wave. *Invest Ophthalmol Vis Sci*. 1994;35:635–645.
42. Machida S, Toba Y, Ohtaki A, Gotoh Y, Kaneko M, Kurosaka D. Photopic negative response of focal electoretinograms in glaucomatous eyes. *Invest Ophthalmol Vis Sci*. 2008;49: 5636–5644.
43. Quigley HA, Brown AE, Morrison JD, Drance SM. The size and shape of the optic disc in normal human eyes. *Arch Ophthalmol*. 1990;108:51.
44. Frishman L, Sustar M, Kremers J, et al. ISCEV extended protocol for the photopic negative response (PhNR) of the full-field electroretinogram. *Doc Ophthalmol*. 2018;136:207–211.
45. Kiszkielis M, Lubinski W, Penkala K. The photopic negative response as a promising diagnostic tool in glaucoma. A review. *Klin Ocz*. 2012;114:138–142.

Investigative Ophthalmology & Visual Science

Downloaded from arvojournals.org on 05/13/2019